batteries

MDPI

Article

Study of the Suitability of Corncob Biochar as Electrocatalyst for Zn–Air Batteries

Nikolaos Soursos [1], Theodoros Kottis [1], Vasiliki Premeti [1], John Zafeiropoulos [2], Katerina Govatsi [3], Lamprini Sygellou [4], John Vakros [1,*], Ioannis D. Manariotis [5], Dionissios Mantzavinos [1] and Panagiotis Lianos [1,*]

1 Department of Chemical Engineering, University of Patras, 26500 Patras, Greece; up1060051@ac.upatras.gr (N.S.); up1060033@upnet.gr (T.K.); up1060107@ac.upatras.gr (V.P.); mantzavinos@chemeng.upatras.gr (D.M.)
2 School of Science and Technology, Hellenic Open University, Parodos Aristotelous 18, 26335 Patras, Greece; jzafeirop@eap.gr
3 Laboratory of Electron Microscopy and Microanalysis, School of Natural Sciences, University of Patras, 26500 Patras, Greece; kgovatsi@upatras.gr
4 Foundation of Research and Technology, Institute of Chemical Engineering Science (FORTH/ICE-HT), Stadiou Str. Platani, P.O. Box 1414, 26500 Patras, Greece; sygellou@iceht.forth.gr
5 Environmental Engineering Laboratory, Department of Civil Engineering, University of Patras, University Campus, 26500 Patras, Greece; idman@upatras.gr
* Correspondence: vakros@chemistry.upatras.gr (J.V.); lianos@upatras.gr (P.L.)

Abstract: There has been a recent increasing interest in Zn–air batteries as an alternative to Li-ion batteries. Zn–air batteries possess some significant advantages; however, there are still problems to solve, especially related to the tuning of the properties of the air–cathode which should carry an inexpensive but efficient bifunctional oxygen reduction (ORR) and oxygen evolution (OER) reaction electrocatalyst. Biochar can be an alternative, since it is a material of low cost, it exhibits electric conductivity, and it can be used as support for transition metal ions. Although there is a significant number of publications on biochars, there is a lack of data about biochar from raw biomass rich in hemicellulose, and biochar with a small number of heteroatoms, in order to report the pristine activity of the carbon phase. In this work, activated biochar has been made by using corncobs. The biomass was first dried and minced into small pieces and pyrolyzed. Then, it was mixed with KOH and pyrolyzed for a second time. The final product was characterized by various techniques and its electroactivity as a cathode was determined. Physicochemical characterization revealed that the biochar had a hierarchical pore structure, moderate surface area of 92 m^2 g^{-1}, carbon phase with a relatively low sp^2/sp^3 ratio close to one, and a limited amount of N and S, but a high number of oxygen groups. The graphitization was not complete while the biochar had an ordered structure and contained significant O species. This biochar was used as an electrocatalyst for ORR and OER in Zn–air batteries where it demonstrated a satisfactory performance. More specifically, it reached an open-circuit voltage of about 1.4 V, which was stable over a period of several hours, with a short-circuit current density of 142 mA cm^{-2} and a maximum power density of 55 mW cm^{-2}. Charge–discharge cycling of the battery was achieved between 1.2 and 2.1 V for a constant current of 10 mA. These data show that corncob biochar demonstrated good performance as an electrocatalyst in Zn–air batteries, despite its low specific surface and low sp^2/sp^3 ratio, owing to its rich oxygen sites, thus showing that electrocatalysis is a complex phenomenon and can be served by biochars of various origins.

Keywords: biochar; corncob; electrocatalysis; Zn–air batteries; ORR; OER

Citation: Soursos, N.; Kottis, T.; Premeti, V.; Zafeiropoulos, J.; Govatsi, K.; Sygellou, L.; Vakros, J.; Manariotis, I.D.; Mantzavinos, D.; Lianos, P. Study of the Suitability of Corncob Biochar as Electrocatalyst for Zn–Air Batteries. *Batteries* **2024**, *10*, 209. https://doi.org/10.3390/batteries10060209

Academic Editors: Hao Liu and Dino Tonti

Received: 15 April 2024
Revised: 31 May 2024
Accepted: 14 June 2024
Published: 16 June 2024

1. Introduction

An interesting and realistic alternative to Li batteries is Zn batteries. Zn batteries exhibit some advantages, for example, the abundance and lower cost of Zn compared to Li,

the easier treatment of Zn, and the fact that Zn batteries are environmentally friendly. Zinc can be employed directly as an anode in contrast to other metals. The Zn batteries are more stable and safer, with a longer lifespan, and they use aqueous electrolytes, which makes them more attractive than other types of batteries, which need more complex electrolytes. Zinc metal has a redox potential of −0.76 V vs. RHE, is relatively resistant to oxidation in an aqueous environment, and it is easy to reverse the oxidation of Zn to Zn^{2+}. Also, it has been reported to reach a significant specific capacity (820 mAh g^{-1}) [1–3]. A comprehensive approach for the Zn-ion batteries includes not only the Zn anode but also the electrolyte [4] and the cathode materials [5]. This is also valid for other types of batteries like Li-S batteries [6]. In such cases, the electrolyte can determine the efficiency of the battery [7].

Zn–air batteries, the most popular among Zn batteries, function with aqueous electrolytes while Zn metal itself makes the anode electrode. For this reason, cathode materials make the difference in Zn–air batteries. Thus, it is not surprising that the effort of the scientific community on the Zn–air batteries [8–12] is ever-increasing, but there remains a focus on the quality of the cathode. Despite its great advantages, Zn–air battery performance is sensitive to ambient conditions while, as already said, an advanced design is necessary for the air electrode. Although the Zn–air battery has the maximum discharge capacity among zinc-based batteries, it has a limited power output, again mainly due to the inadequate performance of air electrodes [13], and it is not fully competitive with other types of batteries [14].

In addition, Zn–air batteries have an unsatisfactory life cycle and energy conversion efficiency. This is again due to the air–cathode. The two important electrochemical reactions on the air–electrode (cathode) are the ORR during discharging and the OER during charging [3]. These two reactions follow multiple mechanisms and generally have slow kinetics and high overpotential. The ORR at the air (cathode) electrode is of great importance in these batteries. The anode (metal Zn in our case) is oxidized, and the electrons should react on the cathode with oxygen in a very efficient way; otherwise, the electrons are accumulated and reduce water to produce H_2.

The ORR can follow $2e^-$ or $4e^-$ kinetics which are shown by the following reactions, written for an alkaline electrolyte [15]:

$$O_2 + 2e^- + 2H_2O \rightarrow H_2O_2 + 2OH^- \quad (1)$$

$$O_2 + 4e^- + 2H_2O \rightarrow 4OH^- \quad (2)$$

OER and ORR are significant for the performance of Zn–air batteries, but are very challenging due to their complexity, slow kinetics, and high overpotential. To overcome these problems, a new highly reversible bifunctional electrocatalyst should be synthesized. Generally, these criteria demand electrodes with transition metals, although carbon materials are part of the electrocatalyst [16,17].

The four-electron semi-reaction is obviously preferable, since $4e^-$ are then consumed, but it demands a powerful electrocatalyst. In recent days, the trend for less costly, greener, and more environmentally friendly agents attracts the focus of new eco-friendly materials used in plenty of applications, including Zn–air batteries, where they have been applied as electrocatalysts on the cathode electrode. Such electrocatalysts should be bifunctional and active for both ORR and OER, in order to recharge the battery. Thus, the electrocatalyst should have electrical conductivity, high active surface area, and porosity with hierarchical structure and surface groups that can participate in the interfacial electro-reactions [7,18,19]. Among the recently studied possible candidates for electrocatalysis, biochar has several advantages. It possesses the above-described characteristics, it can be easily produced from different types of biomass, and it can also be considered as a by-product, or even waste, of the pyrolysis of biomass for the production of liquid and air fuels. Biochar is a carbonaceous residue from the pyrolysis of raw biomass in the absence of oxygen or in a limited oxygen atmosphere. Generally, it has a significant specific surface area (SSA) and, depending on the pyrolysis conditions, various oxygen-containing surface groups. The

pyrolysis graphitizes the carbon phase giving biochar the required electrical conductivity, while during pyrolysis the gases produced help to increase the porosity and the SSA of the final biochar. Furthermore, biochar can be prepared from any kind of waste biomass, both from plants and animals [20–23].

Biochar can be easily post-treated chemically with acidic or basic compounds to improve its physicochemical properties. The post-treatment can be performed with or without pyrolysis [24–28]. In the case of post-treatment without a second pyrolysis step, the biochar surface reacts with added acid or base and significant changes can be detected in the surface groups, the acidity, and the SSA of the biochar [24]. More intense changes occur when the post-treatment is followed by a second pyrolysis. In these cases, for example, in pyrolysis of an already prepared biochar abundantly mixed with KOH, which is a process similar to the production of activated carbons, the graphitic layers are affected, and K ions intercalate among them. This process increases SSA since a high quantity of volatile compounds is then released. Thus, the final product has a hierarchical pore distribution. Among others, KOH also reacts and dissolves lignin [20,22,23,29,30].

Biochar, as a carbonaceous material, exhibits a significant amount of oxygen-containing surface sites, while other heteroatoms, such as N, P, and S can be detected. These atoms usually favour the electrocatalytic activity and have a synergistic effect with the carbon conductive phase. In this view, doping with different heteroatoms has been applied as a route for improving the electrocatalytic activity. The doping is not only limited to non-metal atoms, like N and S, but also transition metal ions were used [31–33].

Biochar electrode studies have become very popular in the last few years since the use of an abundant, inexpensive material originating from residual biomass is very attractive. Some applications like direct carbon fuel cells and supercapacitors have been reported [34–38]. The high SSA is a desirable characteristic but not crucial for the efficiency of the electrode. For example, four different carbon materials, Vulcan XC-72R, carbon nanotubes, graphene, and biochar were used as supports for electrocatalysts in fuel cell applications and it has been reported that other characteristics, like the crystalline phase and the point of zero charge of the carbon material, affect the interactions between the carbon and metal phase and consequently the electrocatalytic activity [39]. Also, biochar from spent malt rootlets untreated or with various chemical treatments was used as supercapacitors [40] or as an electrode for the production of H_2O_2 [41], and the influence of the SSA was not significant.

Also, in a recent study, data about electrodes from wheat were collected and discussed [42] where the SSA values vary considerably with no direct correlation with the electroactivity of the biochar. A more detailed study concerning the influence of the SSA on the properties of activated graphene as a supercapacitor points out that other parameters like the milling procedure and pyrolysis temperature resulted in a better electrode performance despite a decrease in the SSA by 30% [43].

In this study, we have examined the electrocatalytic functionality of biochar from corncobs. Corncobs, a waste produced in high quantities, are usually burned, although more than 1 million tons are disposed of every year [43]. Corncobs are one of the few biomass types with a high hemicellulose composition, usually between 26% and 36% and sometimes even more, which differentiates them from other residual biomasses [44,45]. Cellulose and lignin are the main components of the carbonaceous phase, which do not contribute to electric conductivity.

Biochar from corncobs has been prepared and used in many other, non-electrochemical applications. Corncob biochar is not so popular, since it demonstrates a low SSA of some $m^2\ g^{-1}$ and a low concentration of non-metal heteroatoms. Despite these two rather disadvantageous characteristics and the fact that the presently used biochar did not contain any metal or non-metal groups, we proceeded to make activated biochar from corncobs in order to study its performance as an electrocatalyst in Zn–air batteries.

Our purpose was to investigate the possibility of a biochar originating from biomass with high hemicellulose content and to report the pristine activity of the carbon phase.

Finally, we want to compare the present biochar with two previously reported biochars rich in lignin.

Indeed, in a recent article [38] we reported the electrochemical behaviour of two KOH-activated biochars from olive tree twigs and spent malt rootlets. Both had high lignin content, and the treatment with KOH did result in a high SSA. It was found that the biomass origin exhibits a minor effect on the electrochemical behaviour of the biochar since the second pyrolysis step homogenized the properties of the two biochars. This may also be valid for other biochars of other origins, especially biochars from biomass rich in lignin, such as the present one. In this sense, it is interesting to study the electrochemical characteristics of a biochar prepared under the same preparation conditions but originating from corncobs, despite its other less desirable characteristics and to support a conclusion that the biomass origin is not the crucial factor for the determined electro-activity. Thus, in this work, biochar has been made from corncobs and subsequently activated with KOH under pyrolysis, characterized with different physicochemical techniques, finally used as a cathode electrocatalyst in Zn–air batteries, and tested for its ORR and OER capacity.

2. Materials and Methods

2.1. Biochar and Electrode Preparation

All reagents used were of analytical grade and purchased from Sigma-Aldrich (St. Louis, MO, USA) except for the carbon cloth (CC) (Fuel Cell Earth, Wobum, MA, USA) and carbon black (CB) (Cabot Corporation Vulcan XC72, Billerica, MA, USA). The biochar was prepared from corncobs under pyrolysis with a limited O_2 atmosphere (20% O_2) and activated with a second pyrolysis step, after mixing with KOH in a ratio of KOH/biochar = 3/1. The activation temperature was 850 °C. More details about the biochar preparation and activation can be found in [38].

The collected biochar was used to prepare electrodes through deposition on CC with a dimension of 1 cm × 1 cm with the same procedure as in [38]. The same procedure was followed for the preparation of the CB/CC electrode by replacing the biochar with carbon black. Furthermore, a Pt-modified biochar electrode was made by adding Pt, according to the following procedure: Around 50 mg of sodium tetrachloroplatinate was solubilized in a mixture of 1 mL isopropanol with 1 mL acetone. A carbon cloth electrode carrying biochar, as above, was placed on a hot plate and the tetrachloroplatinate solution was drop-casted over the whole area of the biochar. Then, the electrode was again annealed at 340 °C.

2.2. Physicochemical Characterizations

The physicochemical characterization of biochar was performed using Scanning Electron Microscopy (SEM) (JEOL, JSM-6300, JEOL USA, Inc., Peabody, MA, USA), X-ray Photoelectron Spectroscopy (XPS) (SPECS Phoibos 100-1D-DLD, SPECS Surface Nano Analysis GmbH, Berlin, Germany), porosimetry, (Tristar 3000 porosimeter, Micromeritics, Norcross, GA, USA), X-ray diffraction (XRD) (Bruker D8 (Billerica, MA, USA)), Fourier-transform infrared (FTIR) (Perkin Elmer Spectrum RX FTIR system Waltham, MA, USA) and Raman spectroscopy (Jobin-Yvon Horiba LabRam-HR, Lille, France). Details can be found in [38].

2.3. An Electrochemical Characterization of the Electrodes and Construction and Operation of the Zn–Air Battery

All electrochemical measurements were carried out with an Autolab potentiostat PGSTAT128N (Utrecht, The Netherlands) according to the procedures described in [38].

Zn–air batteries were constructed using a Zn foil (Sigma-Aldrich, St. Louis, MO, USA) anode and a biochar/CC or CB/CC cathode electrode, with a 5 mm distance between the two electrodes, and 5 M of NaOH containing 0.2 M ZnO as the electrolyte [12].

3. Results and Discussion

3.1. Physicochemical Characterization of the Biochar

Figure 1 shows the SEM images of the material. Interestingly, the SEM images reveal a hierarchical porous structure for the corncob biochar.

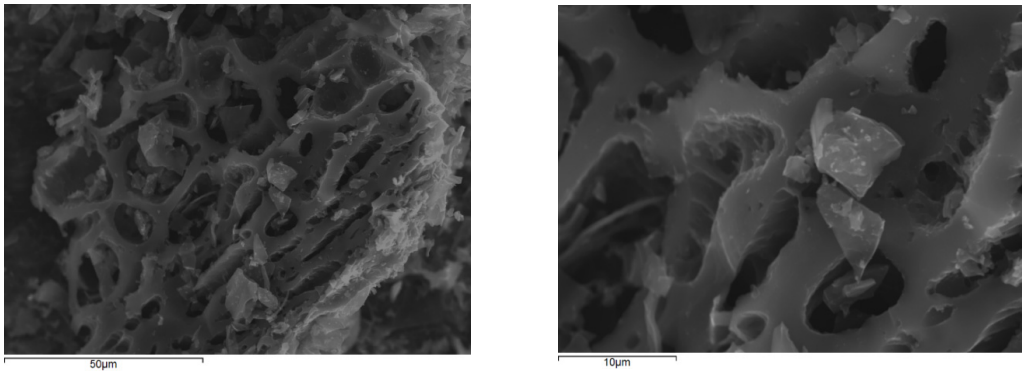

Figure 1. SEM images of corncobs biochar powders after KOH treatment.

The EDX analysis presented in Table 1 confirms that biochar has a high C and O content as expected. K was found at a low concentration as a result of the wash and filtration after the activation treatment. Some traces of Mg, Si, and P were detected while the absence of N and S is possibly due to the extensive pyrolysis.

Table 1. EDX results for the corncob biochar used.

Element	Atoms (%)
C	90.9
O	7.9
K	0.8
Mg	0.1
Si	0.05
P	0.25

A more detailed analysis of the surface was performed with XPS. The XPS survey scan, presented in Figure 2, shows that P was not detected on the surface of the biochar and only traces of Si and Mg were detected. C and O are the main surface elements, while small quantities of K are also present.

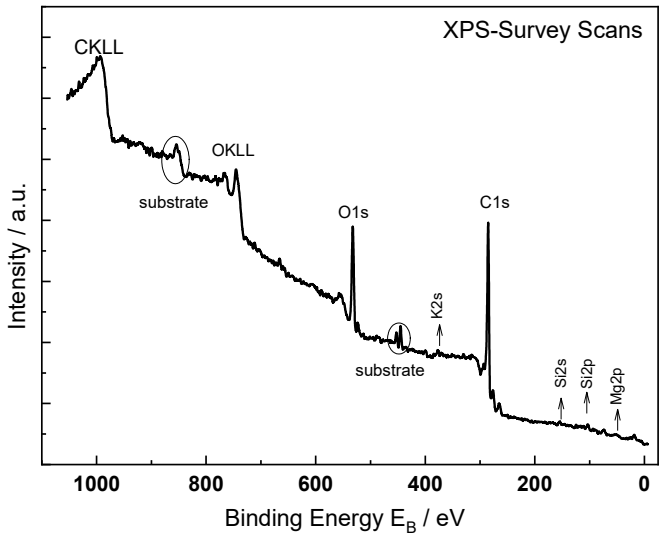

Figure 2. XPS Survey scans of the biochar studied. The Indium foil substrate is marked.

The % surface atomic concentration, presented in Table 2, of each element was calculated from the area of the C1s, O1s, K2p, Si2p, Ca2p, and Mg2p peaks taking into account the relative sensitivity factors.

Table 2. % surface atomic concentration of the corncob biochar from XPS analysis. Data were recorded with a 0.5% error.

XPS Peak	Eb [eV]	Atomic Concentration (%)
C1s	284.5	76.2
Ca2p	347.7	traces
O1s	532.5	17.4
K2p	293.0	1.1
Si2p	103.2	2.8
Mg2p	51.5	2.5

The location of each XPS peak is also presented in Table 2. Interestingly, the location of O1s is at 532.5 eV and this can be attributed mainly to O atoms in C-O bonds, since carbonates and metal hydroxides develop peaks at about 531 eV [46,47].

Comparing Tables 1 and 2, it can be seen that the surface of biochar is enriched in O. probably due to the surface oxidation. Also, a small enrichment of the surface can be detected for K, different than expected since K intercalates above graphitic layers. This is the first evidence that the activation process does not have the desirable effect on the surface characteristics of the biochar. The oxidation of the surface results in different C species and not only graphitic carbon.

Figure 3 shows the combined XPS spectral window of the C1s and K2p peaks. The C1s peak is deconvoluted into carbon (sp^2 and sp^3) and carbon–oxygen bonds with the peak components shown in different colours and the assignments shown in the inset of this figure. The K2p peaks consist of the peaks for $K2p_{1/2}$ and $K2p_{3/2}$.

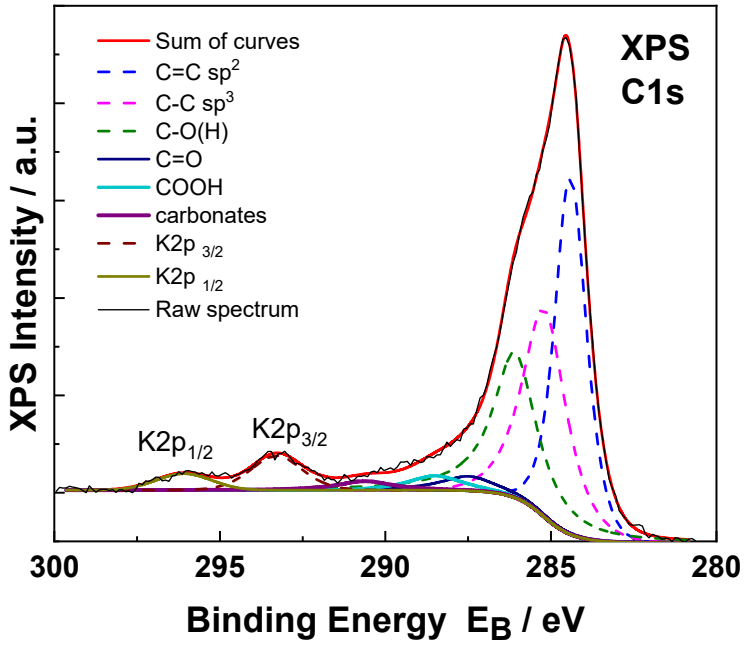

Figure 3. Combined C1s-K2p XPS spectral window for corncob biochar. The C1s peak is deconvoluted into carbon–carbon and carbon–oxygen bonds, while the K2p doublet ($K2p_{1/2}$ and $K2p_{3/2}$) is also present.

The speciation of each carbon surface species is presented in Table 3. Two-thirds of carbon species are non-oxidized, while the rest are oxidized carbon species, 7.5% of which are highly oxidized. The sp^2/sp^3 ratio in this study is slightly above one, one of the lower

values generally reported for different biochars. This ratio is important concerning the ORR activity [48]. In a recent study, it was found that this ratio increases with the pyrolysis temperature, while it is well correlated with the ORR activity. Since sp^2 carbon is related to the C=C bonds and thus with electric conductivity, it is logical that this ratio plays an important role in electrochemical processes [38,48].

Table 3. % Component concentration of C1s XPS peaks of the biochar studied.

Eb (eV)	Assignments	Biochar (±0.5)
284.4 ± 0.1	C-C sp^2	35.9
285.3 ± 0.1	C-C sp^3	30.1
286.2 ± 0.2	C-O(H)	26.2
287.8 ± 0.2	C=O	3.6
289.0 ± 0.2	COOH	2.9
290.5	carbonates	1.9

The adsorption–desorption isotherm is presented in Figure 4a. The shape of the curve is type IV with an H3 hysteresis loop according to IUPAC, suggesting that the material has macropores that are not completely filled with N_2 and a limited amount of non-uniform mesopores. Macropores are also detected with the SEM images. Finally, the biochar also has a portion of micropores as the N_2 amount adsorbed in low P/Po is significant. The pore size distribution is presented in Figure 4b. As can be seen, the majority of the pores are in micropore and macropore regions and only a small amount of mesopores can be detected. The SSA was found to be significantly low, at 92 $m^2\ g^{-1}$, i.e., ten times lower than expected compared to other activated biochars. Generally, biochar from corncobs exhibits a very small SSA of a few $m^2\ g^{-1}$, and only in a few works, the SSA is higher than 100 $m^2\ g^{-1}$ [48,49]. This low SSA of the pristine biochar and the high amount of cellulose and hemicellulose may explain why the activation procedure with KOH is not efficient to give high values of SSA in the activated biochar. The influence of a base in raw biomass is limited to lignin content, while cellulose and hemicellulose react with acids to be dissolved. This is also valid for the carbonaceous phase of the pristine biochar [24]. In our case, corncobs with high amounts of hemicellulose produce pristine biochar with low SSAs. Thus, treatment with KOH does not affect, to a high extent, the carbonaceous phase. During the pyrolysis procedure, KOH was melted at temperatures above 406 °C, helping the reaction with lignin and the carbon phase originating from lignin. On the other hand, hemicellulose is inactive in basic solutions and requires acidic solutions to be dissolved.

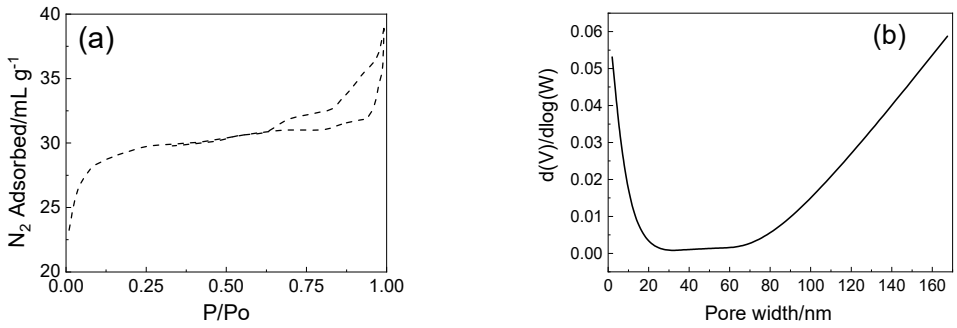

Figure 4. The adsorption–desorption isotherms (**a**) and pore size distribution (**b**) for the biochar studied.

The XRD pattern of the biochar is presented in Figure 5. The XRD patterns of the biochar show two main broad peaks centred at 24° and 43.6°. The pattern is typical of a disorder of amorphous graphitic material. The first peak corresponds to C(002), typical of the amorphous graphitic phase [50], while the second is due to C(100). This peak describes C in sp^2 hybridization, i.e., the carbon species that are responsible for the electric conductivity of the biochar [51]. It is interesting that no other well-formed peaks

for inorganic compounds are detected, in contrast to a previous study [38], especially peaks that correlate to potassium salts, pointing out that the activation process was not so successful in this biochar. This is in accordance with XPS and EDX results, where the amount of K is rather low.

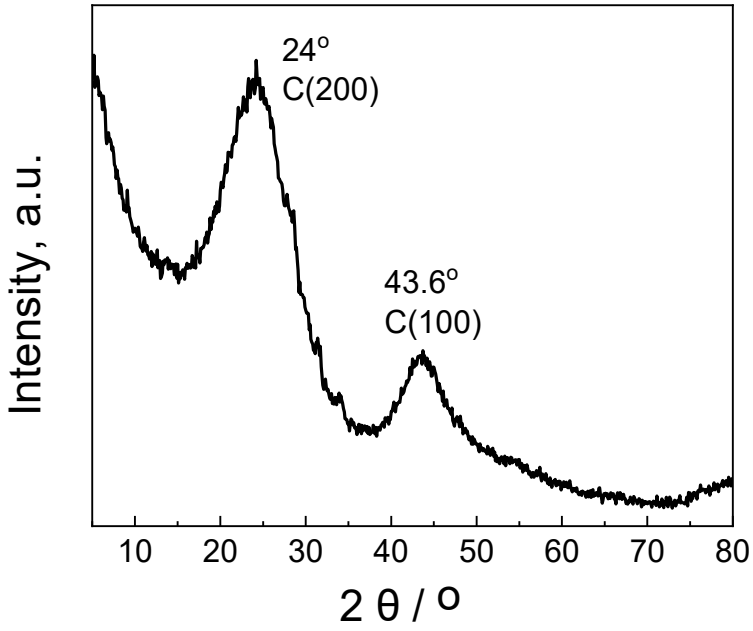

Figure 5. XRD pattern of activated biochar from corncobs.

The FTIR spectrum of the biochar is presented in Figure 6. The main peak is the intense band centered at 1384 cm^{-1} and can be attributed to carbonates. Interestingly, this peak is located between the peak in pure potassium carbonate (1353 cm^{-1}) and the hydrated magnesium carbonate (1417 cm^{-1}), thus suggesting that the carbonate species interact with the detected cations [52]. There are also two other broad bands, at 1092 cm^{-1} and 3422 cm^{-1}. These bands are related to the O-containing groups of the biochar. The first is due to C–O bonds, while the second is due to –OH groups or even adsorbed water molecules [53–55].

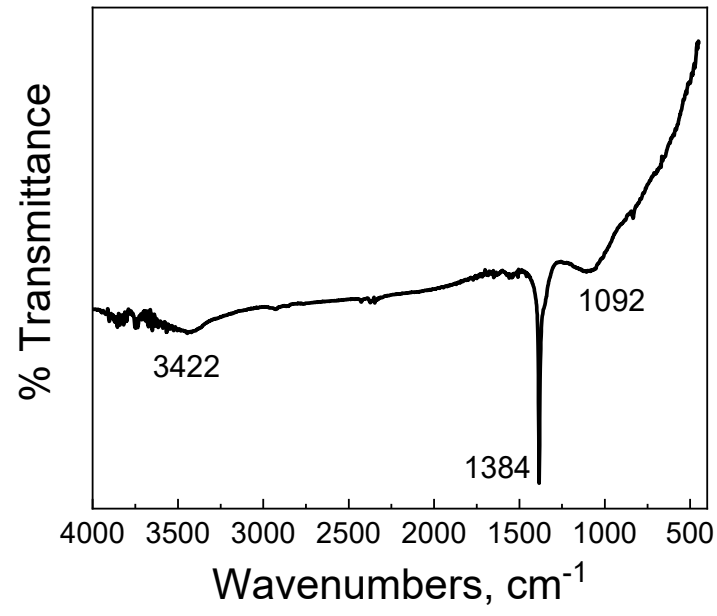

Figure 6. FTIR spectrum of biochar studied.

The Raman spectrum of the activated biochar is presented in Figure 7. As can be seen, the spectrum is typical of disordered carbon materials. There are two main peaks centered at 1349 and 1591 cm^{-1}, with a broad band above 2500 cm^{-1}. The first peak is the D band which described the disordered carbon structures of the biochar, specifically the aromatics with no less than 6 rings but fewer rings than graphite. The second band, the G band, is associated with sp^2-hybridized carbon atoms in graphitic carbon layers, C=C on the aromatic ring, and amorphous carbon. The G band indicates the presence of organized sp^2 domains, while the D band is related to defects associated with the breaking of the hexagonal symmetry of the carbon atoms [39,56–58]. The ratio I_D/I_G is related to the crystallinity of biochar. In our case, the ratio I_D/I_G was found equal to 1.06. Values around one denote that the biochar has an adequate degree of carbon ordering, but also a sufficient number of functional groups. These groups increase the inter-spacing between carbon layers. It is interesting that in our case the absence of other bands in the spectrum denotes that the biochar is not a highly disordered material. Also, no band was detected at about 1260 cm^{-1}, where the S band can be detected. The S band is due to C_{alkyl}-C_{aryl} and is related to the sp^3 carbon species. The absence of this band suggests that the biochar has a significant amount of O species [59].

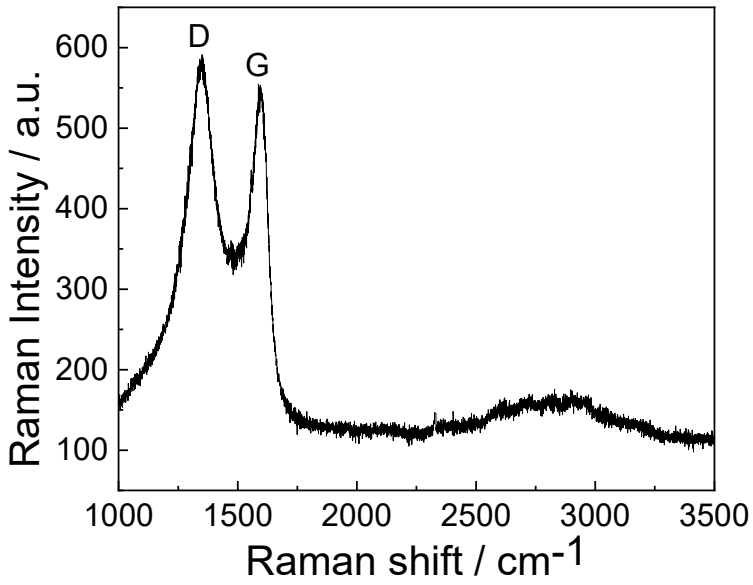

Figure 7. Raman spectrum of biochar studied.

3.2. Electrocatalytic Properties of the Corncob Biochar

The water oxidation, i.e., OER, and the ORR capacity of the corncob biochar electrode have been examined in comparison with the Pt/biochar/CC electrode and the CB/CC electrode. The results are presented in Figure 8a (oxidation) and Figure 8b (reduction). The distinction between biochar and CB electrodes is obvious in both oxidation and reduction. Even though the standard CB/CC carbon electrode is functional in both processes, an important advantage is offered by the present corncob biochar electrode. Indeed, in that case, both water oxidation and oxygen reduction took place at lower voltages than in the case of carbon black, indicating the advantage of using biochar as an electrode. The addition of Pt had a rather limited effect. This indicates that the biochar electrode can practically function well by itself, and the presence of platinum is not necessary.

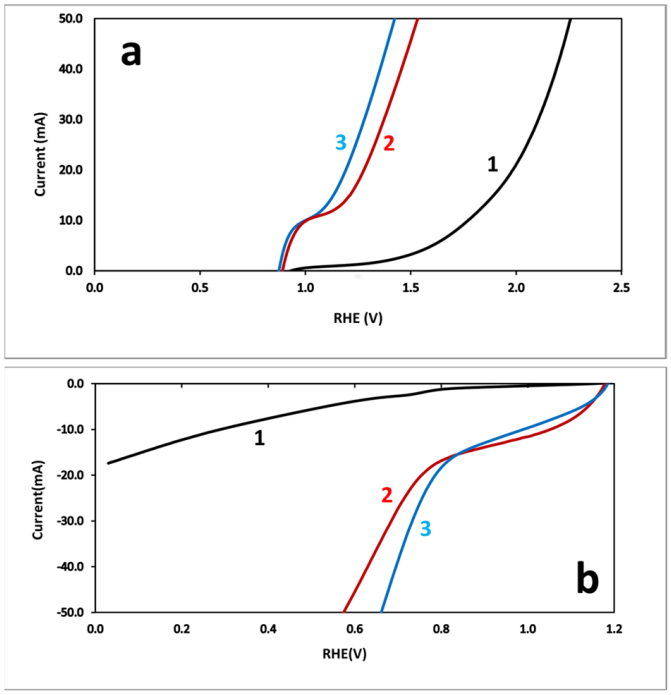

Figure 8. Linear sweep voltammetry data in a 3-electrode reactor with (1) CB/CC; (2) biochar/CC; and (3) Pt/biochar/CC as the working electrode, Pt wire as the counter, and Ag/AgCl as the reference electrode. The electrolyte was an oxygen-saturated 0.5 M of NaOH. Data were plotted against the RHE electrode. (**a**) Data were obtained in the direction of increasing voltage (oxidation) and (**b**) in the direction of decreasing voltage (reduction).

The oxidation activity of the corncob biochar is very close to that observed in a previous study [38]. The water oxidation threshold is slightly above 1.25 V vs. RHE as was the case of the two previously studied biochars [38], which was significantly lower than that of the CB electrode. Interestingly, these two biochars had a much higher sp^2/sp^3 ratio, i.e., around 3.6, while the biochar in this study had a ratio of around 1. These differences in C hybridization can be attributed to the raw biomass. Corncobs rich in hemicellulose and cellulose have fewer aromatic structures in contrast to lignin, and this difference may explain the lower ratio. This ratio was also influenced by the pyrolysis temperature since higher temperatures increase the aromaticity of the biochar; however, since the pyrolysis temperature is the same for all three biochars, then the raw biomass can be considered as the key factor for the low value of the sp^2/sp^3 ratio in the case of corncobs.

3.3. Application in the Construction of a Zn–Air Battery

Zn–air batteries were actually made using corncob biochar/CC as cathode electrodes. Figure 9a shows the corresponding potential vs. current density and power density vs. current density curves. The battery reached an open-circuit voltage of about 1.4 V. This value was stable over a period of several hours, as seen in Figure 9b. The short-circuit current was 142 mA cm^{-2} and the maximum power density was 55 mW cm^{-2}. By taking into account the fact the carbon material should act both as an ORR and OER electrocatalyst, the cell underwent charge–discharge cycles. We are reminded at this point that during discharging, oxygen is reduced at the cathode electrode, while during charging, water is oxidized and oxygen evolves also at the cathode electrode. Figure 10 shows the charge–discharge cycles for a Zn–air battery operating with either biochar/CC or CB/CC cathode electrodes, for comparison. In the case of the CB/CC, the battery discharge operated at 1.0 V while more than 2.7 V was necessary to charge the battery at a constant current of 10 mA. In the case of biochar (corncob)/CC, the corresponding values were 1.2 and 2.1 V. This result is very interesting and shows that corncob biochar can be a successful electrocatalyst

for Zn–air batteries. It is seen that a battery running with corncob biochar can yield a higher voltage for a given current and spends much less energy to be charged than when it is running with a standard Vulcan XC72 catalyst. This is an important technological advantage, in view of the availability and easy processing of corncob wastes. The findings shown in Figure 10 are in accordance with those of Figure 8.

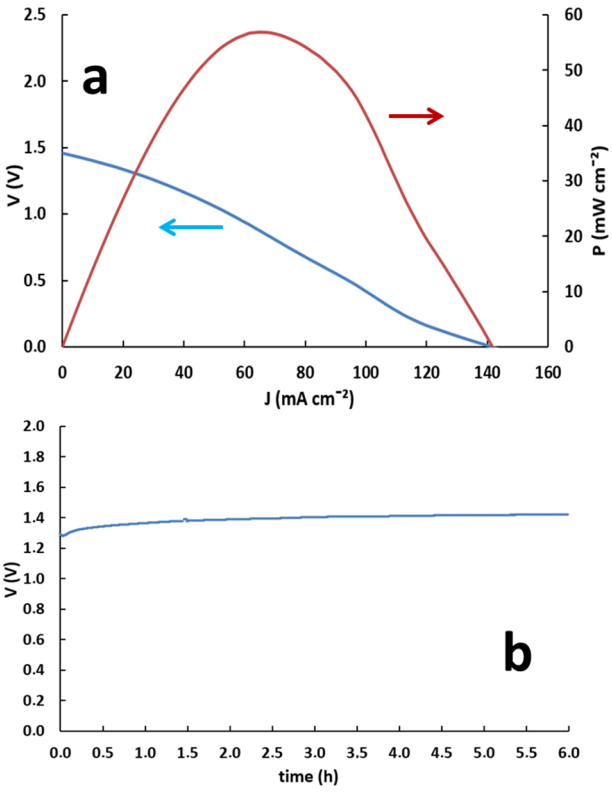

Figure 9. (**a**) Polarization curve (blue line) and power density curve (red line) for Zn–air battery made with corncob biochar as electrocatalyst. (**b**) Open-circuit voltage potentiometry for the same battery.

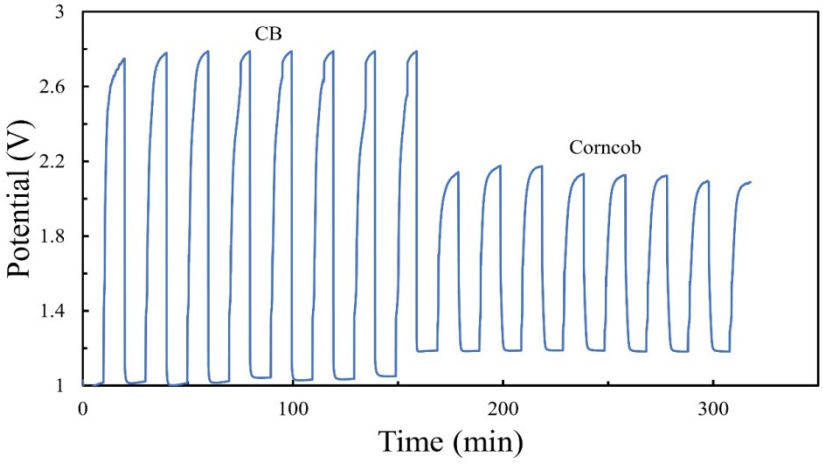

Figure 10. Galvanostatic charge–discharge cycles for a Zn–air battery carrying a cathode electrode loaded with either CB or biochar electrocatalyst. The current was 10 mA. The active sizes of both the anode and cathode were 1 cm^2 each.

4. Conclusions

Corncob was used as raw biomass for the preparation of activated biochar. The biochar exhibited moderate SSA but achieved a hierarchical porous structure and preserved a high

amount of O active groups. The carbon phase was rich in sp^3 species, despite the high pyrolysis temperature. This can be attributed to the speciation of the raw biomass and the high amount of hemicellulose and cellulose. The low content of lignin in raw biomass increased the difficulty of releasing volatile species; thus, the SSA remained low, and the aromatization process was obstructed. In spite of these undesirable characteristics, the electrochemical behaviour of the biochar was interesting. Corncob biochar has been successfully employed as both ORR and OER in Zn–air batteries. Despite the fact that this material fails to attain a high SSA, it seems that the large percentage of oxygen active sites enhances its performance as an electrocatalyst. The above results verify the fact that electrocatalysis is a complex phenomenon and can be served by biochars of various origins.

Author Contributions: Investigation, N.S., T.K., V.P. and J.Z.; investigation, data curation, validation, K.G. and L.S.; resources, I.D.M., D.M. and P.L.; supervision, P.L; writing—original draft preparation, J.V. and P.L.; writing—review and editing, J.V., D.M. and P.L. All authors have read and agreed to the published version of the manuscript.

Funding: This research received no external funding.

Data Availability Statement: The raw data supporting the conclusions of this article will be made available by the authors upon reasonable request.

Conflicts of Interest: The authors declare no conflicts of interest.

References

1. Hong, X.; Deng, C.; He, J.; Liang, B.; Wang, G.; Tu, Z. Existing electrochemical activation mechanisms and related cathode materials for aqueous Zn ion batteries. *Energy Conv. Manag.* **2024**, *299*, 117906. [CrossRef]
2. Yu, A.; Zhang, W.; Joshi, N.; Yang, Y. Recent advances in anode design for mild aqueous Zn-ion batteries. *Energy Stor. Mat.* **2024**, *64*, 103075. [CrossRef]
3. Xu, C.; Niu, Y.; Au, V.K.-M.; Gong, S.; Liu, X.; Wang, J.; Wu, D.; Chen, Z. Recent progress of self-supported air electrodes for flexible Zn-air batteries. *J. Energy Chem.* **2024**, *89*, 110–136. [CrossRef]
4. Liu, C.; Xie, X.; Lu, B.; Zhou, J.; Liang, S. Electrolyte strategies toward better zinc-ion batteries. *ACS Energy Lett.* **2021**, *6*, 1015–1033. [CrossRef]
5. Zhou, T.; Zhu, L.; Xie, L.; Han, Q.; Yang, X.; Chen, L.; Wang, G.; Cao, X. Cathode materials for aqueous zinc-ion batteries: A mini review. *J. Colloid. Interf. Sci.* **2022**, *605*, 828–850. [CrossRef] [PubMed]
6. Zhou, C.; Dong, C.; Wang, W.; Tian, Y.; Shen, C.; Yan, K.; Mai, L.; Xu, X. An ultrathin and crack-free metal-organic framework film for effective polysulfide inhibition in lithium–sulfur batteries. *Interdiscip. Mater.* **2024**, *3*, 306–315. [CrossRef]
7. Zhang, L.; Liu, Y.; You, Y.; Vinu, A.; Mai, L. NASICONs-type solid-state electrolytes: The history, physicochemical properties, and challenges. *Interdiscip. Mater.* **2023**, *2*, 91–110. [CrossRef]
8. Li, Y.; Dai, H. Recent advances in zinc–air batteries. *Chem. Soc. Rev.* **2014**, *43*, 5257. [CrossRef] [PubMed]
9. Lianos, P. A brief review on solar charging of Zn–air batteries. *Phys. Chem. Chem. Phys.* **2023**, *25*, 11883–11891. [CrossRef]
10. Wang, C.; Ran, S.; Sun, W.; Zhu, Z. Biomass-derived carbon materials with controllable preparation and their applications in zinc-air batteries: A mini review. *Electrochem. Comm.* **2023**, *154*, 107557. [CrossRef]
11. Sharma, R.; Kumar, H.; Kumar, G.; Sharma, S.; Aneja, R.; Sharma, A.K.; Kumar, R.; Kumar, P. Progress and challenges in electrochemical energy storage devices: Fabrication, electrode material, and economic aspects. *Chem. Eng. J.* **2023**, *468*, 143706. [CrossRef]
12. Katsaiti, M.; Papadogiannis, E.; Dracopoulos, V.; Keramidas, A.; Lianos, P. Solar charging of a Zn-air battery. *J. Power Sources* **2023**, *555*, 232384. [CrossRef]
13. Lionetto, F.; Arianpouya, N.; Bozzini, B.; Maffezzoli, A.; Nematollahi, M.; Mele, C. Advances in zinc-ion structural batteries. *J. Energy Stor.* **2024**, *84*, 110849. [CrossRef]
14. Dong, C.; Zhou, C.; Wu, M.; Yu, Y.; Yu, K.; Yan, K.; Shen, C.; Gu, J.; Yan, M.; Sun, C.; et al. Boosting Bi-Directional Redox of Sulfur with Dual Metal Single Atom Pairs in Carbon Spheres Toward High-Rate and Long-Cycling Lithium–Sulfur Battery. *Adv. Energy. Mater.* **2023**, *13*, 2301505. [CrossRef]
15. Farhan, A.; Qayyum, W.; Fatima, U.; Nawaz, S.; Balčiūnaitė, A.; Kim, T.H.; Srivastava, V.; Vakros, J.; Frontistis, Z.; Boczkaj, G. Powering the Future by Iron Sulfide Type Material (FexSy) Based Electrochemical Materials for Water Splitting and Energy Storage Applications: A Review. *Small* **2024**, 2402015. [CrossRef] [PubMed]
16. Poudel, M.B.; Vijayapradeep, S.; Sekar, K.; Kim, J.S.; Yoo, D.J. Pyridinic-N exclusively enriched CNT-encapsulated NiFe interfacial alloy nanoparticles on knitted carbon fiber cloth as bifunctional oxygen catalysts for biaxially flexible zinc–air batteries. *J. Mater. Chem. A* **2024**, *12*, 10185–10195. [CrossRef]

17. Poudel, M.B.; Logeshwaran, N.; Kim, A.R.; Karthikeyan, S.C.; Vijayapradeep, S.; Yoo, D.J. Integrated core-shell assembly of Ni_3S_2 nanowires and CoMoP nanosheets as highly efficient bifunctional electrocatalysts for overall water splitting. *J. Alloys Compd.* **2023**, *960*, 170678. [CrossRef]
18. He, B.; Deng, Y.; Wang, H.; Wang, R.; Jin, J.; Gong, Y.; Zhao, L. Metal organic framework derived perovskite/spinel heterojunction as efficient bifunctional oxygen electrocatalyst for rechargeable and flexible Zn-air batteries. *J. Colloid. Interf. Sci.* **2022**, *625*, 502–511. [CrossRef] [PubMed]
19. Li, H.; Askari, S.; Wang, J.; Wolff, N.; Behrens, M.; Kienle, L.; Benedikt, J. Nitrogen-doped $NiCo_2O_4$ nanowires on carbon paper as a self-supported air cathode for rechargeable Zn-air batteries. *Int. J. Hydrogen Energy* **2023**, *48*, 26107–26118. [CrossRef]
20. Mishra, R.K.; Mohanty, K. A review of the next-generation biochar production from waste biomass for material applications. *Sci. Total Environ.* **2023**, *904*, 167171. [CrossRef]
21. Rawat, S.; Wang, C.T.; Lay, C.H.; Hotha, S.; Bhaskar, T. Sustainable biochar for advanced electrochemical/energy storage applications. *J. Energy Stor.* **2023**, *63*, 107115. [CrossRef]
22. Miao, W.; Liu, W.; Ding, Y.; Guo, R.; Zhao, J.; Zhu, Y.; Yu, H.; Zhu, Y. Cobalt (iron), nitrogen and carbon doped mushroom biochar for high-efficiency oxygen reduction in microbial fuel cell and Zn-air battery. *J. Environ. Chem. Eng.* **2022**, *10*, 108474. [CrossRef]
23. Venkatachalam, C.D.; Sekar, S.; Sengottian, M.; Ravichandran, S.R.; Bhuvaneshwaran, P. A critical review of the production, activation, and morphological characteristic study on functionalized biochar. *J. Energy Stor.* **2023**, *67*, 107525. [CrossRef]
24. Ntaflou, M.; Vakros, J. Transesterification activity of modified biochars from spent malt rootlets using triacetin. *J. Clean. Prod.* **2020**, *259*, 120931. [CrossRef]
25. Kalampaliki, D.; Jayasingheb, G.D.T.M.; Avramiotis, E.; Manariotis, I.D.; Venieri, D.; Poulopoulos, S.G.; Szpunar, J.; Vakros, J.; Mantzavinos, D. Application of a KOH activated biochar for the activation of persulfate and the degradation of sulfamethoxazole. *Chem. Eng. Res. Des.* **2023**, *194*, 306–317. [CrossRef]
26. Ioannidi, A.A.; Vakros, J.; Frontistis, Z.; Mantzavinos, D. Tailoring the Biochar Physicochemical Properties Using a Friendly Eco-Method and Its Application on the Oxidation of the Drug Losartan through Persulfate Activation. *Catalysts* **2022**, *12*, 1245. [CrossRef]
27. Azargohar, R.; Dalai, A.K. Steam and KOH activation of biochar: Experimental and modeling studies. *Microporous Mesoporous Mater.* **2008**, *110*, 413–421. [CrossRef]
28. Xia, D.; Tan, F.; Zhang, C.; Jiang, X.; Chen, Z.; Li, H.; Zheng, Y.; Li, Q.; Wang, Y. $ZnCl_2$-activated biochar from biogas residue facilitates aqueous As(III) removal. *Appl. Surf. Sci.* **2016**, *377*, 361–369. [CrossRef]
29. Mahbub, M.A.A.; Mulyadewi, A.; Adios, C.G.; Sumboja, A. Sustainable Chicken Manure-derived Carbon as a Metalfree Bifunctional Electrocatalyst in Zn-air Battery. *AIP Conf. Proc.* **2022**, *2652*, 040011. [CrossRef]
30. Tripath, M.; Sahu, J.N.; Ganesan, P. Effect of process parameters on production of biochar from biomass waste through pyrolysis: A review. *Ren. Sustain. Energy Rev.* **2016**, *55*, 467–481. [CrossRef]
31. Lin, X.; Xue, L.; Liu, B.; Qiu, X.; Liu, J.; Wang, X.; Qi, Y.; Qin, Y. Lignosulfonate-assisted in situ synthesis of Co_9S_8–Ni_3S_2 heterojunctions encapsulated by S/N co-doped biochar for efficient water oxidation. *J. Colloid. Interf. Sci.* **2023**, *644*, 295–303. [CrossRef] [PubMed]
32. Wang, J.; Wu, L.; Shen, L.; Zhou, Q.; Chen, Y.; Wu, J.; Wen, Y.; Zheng, J. CoO embedded porous biomass-derived carbon as dual-functional host material for lithium-sulfur batteries. *J. Colloid. Interf. Sci.* **2023**, *640*, 415–422. [CrossRef] [PubMed]
33. Khedulkar, A.P.; Dang, V.D.; Pandit, B.; Bui, T.A.N.; Tran, H.L.; Doong, R. Flower-like nickel hydroxide@tea leaf-derived biochar composite for high-performance supercapacitor application. *J. Colloid. Interf. Sci.* **2022**, *623*, 845–855. [CrossRef] [PubMed]
34. Liu, W.J.; Jiang, H.; Yu, H.Q. Emerging applications of biochar-based materials for energy storage and conversion. *Energy Environ. Sci.* **2019**, *12*, 1751–1779. [CrossRef]
35. Yang, J.; Tang, S.; Mei, W.; Chen, Y.; Yi, W.; Lv, P.; Yang, G. Valorising lignocellulosic biomass to high-performance electrocatalysts via anaerobic digestion pretreatment. *Biochar* **2024**, *6*, 23. [CrossRef]
36. Pérez-Rodríguez, S.; Pinto, O.; Izquierdo, M.T.; Segura, C.; Poon, P.S.; Celzard, A.; Matos, J.; Fierro, V. Upgrading of pine tannin biochars as electrochemical capacitor electrodes. *J. Colloid. Interf. Sci.* **2021**, *601*, 863–876. [CrossRef] [PubMed]
37. Li, C.; Cao, K.; Fan, Y.; Li, Q.; Zhang, Y.; Guo, Z. Kinetically well-matched porous framework dual carbon electrodes for high-performance sodium-ion hybrid capacitors. *J. Colloid. Interf. Sci.* **2023**, *652*, 1356–1366. [CrossRef]
38. Kottis, T.; Soursos, N.; Govatsi, K.; Sygellou, L.; Vakros, J.; Manariotis, I.D.; Mantzavinos, D.; Lianos, P. Biochar from olive tree twigs and spent malt rootlets as electrodes in Zn-air batteries. *J. Colloid. Interf. Sci.* **2024**, *665*, 10–18. [CrossRef]
39. Hasa, B.; Martino, E.; Vakros, J.; Trakakis, G.; Galiotis, C.; Katsaounis, A. The effect of carbon support on the electrocatalytic properties of Pt-Ru catalysts. *ChemElectroChem* **2019**, *6*, 4970–4979. [CrossRef]
40. Vakros, J.; Manariotis, I.D.; Dracopoulos, V.; Mantzavinos, D.; Lianos, P. Biochar from Spent Malt Rootlets and Its Application to an Energy Conversion and Storage Device. *Chemosensors* **2021**, *9*, 57. [CrossRef]
41. Dhawle, R.; Vakros, J.; Dracopoulos, V.; Manariotis, I.D.; Mantzavinos, D.; Lianos, P. Enhancement of the photoelectrochemical production of hydrogen peroxide under intermittent light supply in the presence of an optimized biochar supercapacitor. *Electrochimica Acta* **2022**, *427*, 140846. [CrossRef]
42. Parsimehr, H.; Kazemzadeh, P.; Ehsani, A. Wheat-Based Porous Electrodes for Electrochemical Energy Storage Devices. *ECS Adv.* **2023**, *2*, 020503. [CrossRef]

43. Iakunkov, A.; Skrypnychuk, V.; Nordenström, A.; Shilayeva, E.A.; Korobov, M.; Prodana, M.; Enachescu, M.; Larsson, S.H.; Talyzin, A.V. Activated graphene as a material for supercapacitor electrodes: Effects of surface area, pore size distribution and hydrophilicity. *Phys. Chem. Chem. Phys.* **2019**, *21*, 17901–17912. [CrossRef] [PubMed]
44. Rattanaphaiboon, P.; Homdoung, N.; Tippayawong, N. Production and characterization of corncob biochar for agricultural use. *AIP Conf. Proc.* **2022**, *2681*, 020034. [CrossRef]
45. Gandam, P.K.; Chinta, M.L.; Gandham, A.P.; Pabbathi, N.P.P.; Konakanchi, S.; Bhavanam, A.; Atchuta, S.R.; Baadhe, R.R.; Bhatia, R.K. A New Insight into the Composition and Physical Characteristics of Corncob—Substantiating Its Potential for Tailored Biorefinery Objectives. *Fermentation* **2022**, *8*, 704. [CrossRef]
46. Smith, M.; Scudiero, L.; Espinal, J.; McEwen, J.-S.; Garcia-Perez, M. Improving the deconvolution and interpretation of XPS spectra from chars by ab initio calculations. *Carbon* **2016**, *110*, 155–171. [CrossRef]
47. Lohani, P.C.; Tiwari, A.P.; Muthurasu, A.; Pathak, I.; Poudel, M.B.; Chhetri, K.; Dahal, B.; Acharya, D.; Ko, T.H.; Kim, H.Y. Phytic acid empowered two nanos "Polypyrrole tunnels and transition Metal-(Oxy)hydroxide Sheets" in a single platform for unmitigated redox water splitting. *Chem. Eng. J.* **2023**, *463*, 142280. [CrossRef]
48. Ma, L.-L.; Liu, W.-J.; Hu, X.; Lam, P.K.S.; Zeng, J.R.; Yu, H.-Q. Ionothermal carbonization of biomass to construct sp^2/sp^3 carbon interface in N-doped biochar as efficient oxygen reduction electrocatalysts. *Chem. Eng. J.* **2020**, *400*, 125969. [CrossRef]
49. Budai, A.; Wang, L.; Gronli, M.; Strand, L.T.; Antal, M.J., Jr.; Abiven, S.; Dieguez-Alonso, A.; Anca-Couce, A.; Rasse, D.P. Surface Properties and Chemical Composition of Corncob and Miscanthus Biochars: Effects of Production Temperature and Method. *J. Agric. Food Chem.* **2014**, *62*, 3791–3799. [CrossRef]
50. Qian, L.; Guo, F.; Jia, X.; Zhan, Y.; Zhou, H.; Jiang, X.; Tao, C. Recent development in the synthesis of agricultural and forestry biomass–derived porous carbons for super– capacitor applications: A review. *Ionics* **2020**, *26*, 3705–3723. [CrossRef]
51. Gao, G.; Cheong, L.Z.; Wang, D.; Shen, C. Pyrolytic carbon derived from spent coffee grounds as anode for sodium–ion batteries. *Carbon. Resour. Convers.* **2018**, *1*, 104–108. [CrossRef]
52. Vahur, S.; Teearu, A.; Peets, P.; Joosu, L.; Leito, I. ATR-FT-IR spectral collection of conservation materials in the extended region of 4000-80 cm^{-1}. *Anal. Bioanal. Chem.* **2016**, *408*, 3373–3379. [CrossRef] [PubMed]
53. Kiefer, J.; Stärk, A.; Kiefer, A.; Glade, H. Infrared Spectroscopic Analysis of the Inorganic Deposits from Water in Domestic and Technical Heat Exchangers. *Energies* **2018**, *11*, 798. [CrossRef]
54. Magioglou, E.; Frontistis, Z.; Vakros, J.; Manariotis, I.D.; Mantzavinos, D. Activation of Persulfate by Biochars from Valorized Olive Stones for the Degradation of Sulfamethoxazole. *Catalysts* **2019**, *9*, 419. [CrossRef]
55. Grilla, E.; Vakros, J.; Konstantinou, I.; Manariotis, I.D.; Mantzavinos, D. Activation of persulfate by biochar from spent malt rootlets for the degradation of trimethoprim in the presence of inorganic ions. *J. Chem. Technol. Biotechnol.* **2020**, *95*, 2348–2358. [CrossRef]
56. Nikolaou, S.; Vakros, J.; Diamadopoulos, E.; Mantzavinos, D. Sonochemical degradation of propylparaben in the presence of agroindustrial biochar. *J. Environ. Chem. Eng.* **2020**, *8*, 104010. [CrossRef]
57. Yan, Y.; Manickam, S.; Siva Lester, E.; Wu, T.; Pang, C.H. Synthesis of Graphene Oxide and Graphene Quantum Dots from Miscanthus via Ultrasound-Assisted Mechano-Chemical Cracking Method. *Ultrason. Sonochem.* **2021**, *73*, 105519. [CrossRef] [PubMed]
58. Yang, Y.; Kwon, E.E.; Dou, X.; Zhang, M.; Kim, K.H.; Tsang, D.C.W.; Ok, Y.S. Fabrication of spherical biochar by a two-step thermal process from waste potato peel. *Sci. Total Environ.* **2018**, *626*, 478–485. [CrossRef]
59. Li, X.J.; Hayashi, J.; Li, C.Z. FT-Raman spectroscopic study of the evolution of char structure during the pyrolysis of a Victorian brown coal. *Fuel* **2006**, *85*, 1700–1707. [CrossRef]